Article

Singularity-Free Fixed-Time Adaptive Control with Dynamic Surface for Strict-Feedback Nonlinear Systems with Input Hysteresis

Xuxiang Feng [ID], Jun Chen and Tongyao Niu *

Aerospace Information Research Institute, Chinese Academy of Sciences, No.9 Dengzhuang South Road, Haidian District, Beijing 100094, China; fengxx@aircas.ac.cn (X.F.); chenjun@aircas.ac.cn (J.C.)
* Correspondence: niuty@aircas.ac.cn

Abstract: An adaptive fixed-time dynamic surface tracking control scheme is developed in this paper for a class of strict-feedback nonlinear systems, where the control input is subject to hysteresis dynamics. To deal with the input hysteresis, a compensation filter is introduced, reducing the difficulty of design and analysis. Based on the universal approximation theory, the radial basis function neural networks are employed to approximate the unknown functions in the nonlinear dynamics. On this basis, fixed-time adaptive laws are constructed to approximate the unknown parameters. The dynamic surface technique is utilized to handle the complexity explosion problem, where fixed-time performance is ensured. Moreover, the designed controller can avoid singularities and achieve fixed-time convergence of error signals. Simulation results verify the efficacy of the method developed, where a comparison between the scheme developed with existing results is provided.

Keywords: fixed-time control; novel dynamic surface control; input hysteresis; singularity avoidance; strict-feedback nonlinear systems

1. Introduction

Adaptive control has been investigated in past decades due to its strong robustness and high flexibility. Relevant theories, including finite-time adaptive control [1,2], backstepping control [3], sliding mode control [4–6], and adaptive dynamic programming [7–9], have been successfully applied to nonlinear systems with time-delay [10], circuit systems [11], wind energy systems [12–14], strict-feedback nonlinear systems [15], and multiagent systems [16–18]. Among these theories, backstepping control is a useful tool since it can simplify the design and analysis. Moreover, the development of adaptive backstepping control tends to make control methods with fast responses, high tracking precision, and low computation complexity [19]. However, during the process of adaptive backstepping control, an explosion of complexity is often encountered, which decreases tracking precision and increases computation complexity. To improve tracking control performance, this problem calls for solutions.

In the backstepping procedure, the controller often suffers from an explosion of complexity. That is, with the increase in the system order, repeated differentiation leads to a sharp increase in the computation complexity, which augments the difficulty of the control task. To tackle this issue, dynamic surface control (DSC) was proposed in [20], where first-order filters were introduced and filter states replaced the differentiation of virtual control. With the DSC technique, the complexity explosion problem can be excluded. For example, in [21], DSC was combined with fuzzy logic systems to deal with the control design of nonlinear time-delay systems. Jian et al. proposed an adaptive neural DSC scheme for uncertain stochastic nonstrict-feedback systems [22]. In [23], for pure-feedback nonlinear systems, an adaptive neural DSC approach was developed.

In the real world, fast responses are primary requirements for practical systems in certain situations [24]. For example, when a missile is launched, it must hit the target in a specific time interval. Nevertheless, traditional Lyapunov-theory-based methods can only ensure error signals converge to zero in infinite time, which cannot satisfy this need. To handle this issue, based on finite-time Lyapunov theorem, finite-time adaptive control was proposed [25]. It can ensure the convergence of error signals in a finite time interval, which exceeds traditional Lyapunov-theory-based adaptive control. However, there is a significant drawback to finite-time adaptive control. Specifically, the convergence time depends on the initial states of systems, which restricts the application of finite-time adaptive control. To solve this, fixed-time adaptive control was presented [26]. It is based on finite-time adaptive control to make improvements, where the convergence speed does not rely on the initial conditions of systems. In [27], prescribed performance fixed-time control is combined with neural networks to design controllers for uncertain nonlinear systems. Hu et al. developed a fuzzy adaptive fixed-time tracking control scheme with an event-triggered design for nonlinear systems [28]. In [29], measurement noise suppression and augmented sliding mode observers for hypersonic vehicles are considered simultaneously, where the designed controllers are fixed-time convergent.

In engineering applications, input nonlinearity widely exists in many situations. Common input nonlinearity mainly includes input saturation, input dead-zone, and input hysteresis. Input saturation and input dead-zone nonlinearity have been widely investigated. For instance, in [30], nonlinear systems with input saturation are considered. In [31], the small-gain approach was utilized to tackle systems with input saturation. Min et al. introduced a composite observer for nonlinear systems with input saturation [32]. For unmodeled nonstrict-feedback nonlinear systems, input dead-zone was also taken into consideration via the adaptive fuzzy control method in [33]. Moreover, the input hysteresis nonlinearity needs to be paid enough attention. Zhang et al. combined adaptive prescribed performance control and fuzzy logic systems to handle the input hysteresis [34]. In [35], the effect of the input hysteresis on time-varying delay was considered.

In the above-mentioned results, the DSC method presented in [20–23] fails to achieve fixed-time convergence, and the fixed-time control scheme utilized in [26–29] does not consider the explosion of complexity. Furthermore, the compensation filters are not introduced when handling input hysteresis in [30–35]. To resolve these problems, for strict-feedback nonlinear systems with input hysteresis, fixed-time dynamic surface control has not been investigated, which motivates this paper. The contributions are summarized as follows.

1.1. Contribution

1. In this paper, fixed-time dynamic surface control is presented, where extra nonlinear terms are introduced in the first-order filters to improve the filter error convergence speed. Meanwhile, the adaptive laws can also ensure the fixed-time property of parameter approximation errors, and the singularity problem of the controller is avoided.
2. The input hysteresis is considered in this paper and dealt with by introducing a compensation filter, which can compensate for the loss from the input hysteresis.

1.2. Structure

The rest of this paper is organized as follows. Section 2 provides the background knowledge. In Section 3, the problem is formulated. Section 4 presents the control scheme of this paper, where stability analysis for the strict-feedback nonlinear system with the proposed design is given. Section 5 shows the simulation results, where the effectiveness of the developed approach is verified. In Section 6, a conclusion is drawn.

2. Preliminary Knowledge

Consider a class of strict-feedback nonlinear systems with the following dynamics

$$
\begin{aligned}
\dot{X}_i &= X_{i+1} + F_i(\bar{X}_i), i = 1, \ldots, n - 1, \\
\dot{X}_n &= H(U) + F_n(X), \\
Y &= X_1,
\end{aligned}
\tag{1}
$$

where $X = [X_1 \cdots X_n]^{\mathrm{T}} \in \mathbb{R}^n$, $U \in \mathbb{R}$, $Y \in \mathbb{R}$, $F_i(\cdot) : \mathbb{R}^i \to \mathbb{R}$, $\bar{X}_i = [X_1 \cdots X_i]^{\mathrm{T}} \in \mathbb{R}^n$. Moreover, $H(U)$ denotes the input hysteresis nonlinearity, satisfying the following form

$$
\begin{aligned}
H(U) &= \Lambda_1 U + \Lambda_2 \varsigma, \\
\dot{\varsigma} &= \dot{U}\mathcal{G}(\varsigma, \dot{U}), \varsigma(0) = 0, \\
\mathcal{G}(\varsigma, \dot{U}) &= 1 - \mathrm{sign}(\dot{U})\beta|\varsigma|^{N-1}\varsigma - \chi|\varsigma|^N,
\end{aligned}
\tag{2}
$$

where $\Lambda_1 > 0$, $\Lambda_2 > 0$, $\beta > \chi$, and $\chi > 0$ are constants, and $N > 1$ is a positive integer. The input hysteresis nonlinearity (2) is illustrated in Figure 1.
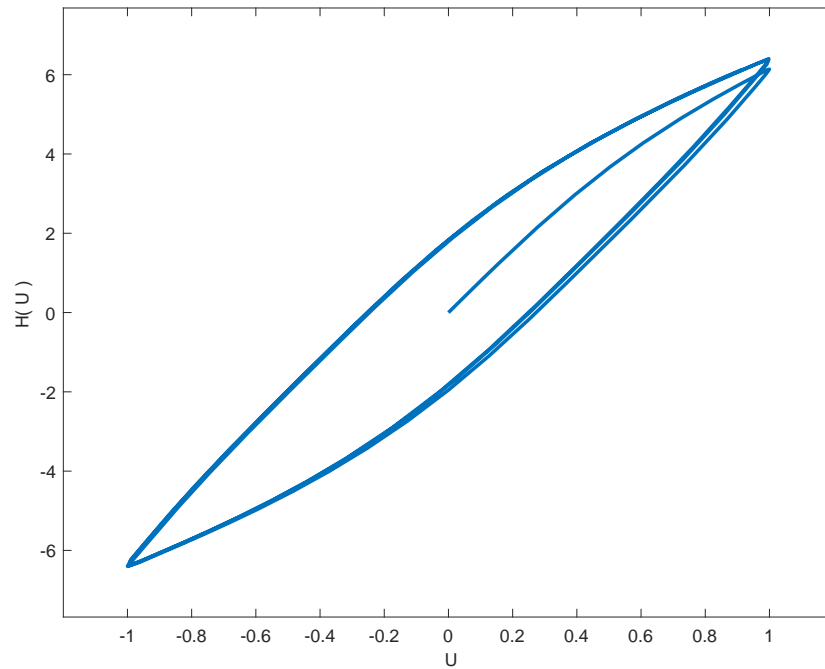

Figure 1. The input hysteresis nonlinearity.

In addition, the reference signal is $X_d(t)$.

Consider radial basis function neural networks (RBFNNs) as

$$
R_{RBF}(Y) = G^{\mathrm{T}}\phi(Y),
\tag{3}
$$

where $G \in \mathbb{R}^m$ and $Y \in \Omega_Y \subset \mathbb{R}^l$ are the vectors of weight and input, respectively. Moreover, the basis function is $\phi(Y) = [\phi_1(Y), \ldots, \phi_m(Y)]^{\mathrm{T}} \in \mathbb{R}^m$ and

$$
\phi_i(Y) = \exp\left(-\frac{[Y - \mu_i]^{\mathrm{T}}[Y - \mu_i]}{2\sigma^2}\right),
\tag{4}
$$

where $\mu_i \in \mathbb{R}^l$ and $\sigma > 0$ correspond to the mean value and variance.

Lemma 1 ([36]). *Given arbitrary parameter $\psi > 0$, sufficiently large node number m, a compact set $\Omega_Y \subseteq \mathbb{R}^l$, and a continuous function $R(Y) : \Omega_Y \to \mathbb{R}$, there is a RBFNN satisfying* (3) *such that*

$$\sup_{Y \in \Omega_Y} \left| R(Y) - G^T \phi(Y) \right| \leq \psi.$$

On account of Lemma 1, we define the optimal weight vector as

$$G^* = \underset{G \in \mathbb{R}^m}{\arg\min} \left\{ \sup_{Y \in \Omega_Y} \left| R(Y) - G^T \phi(Y) \right| \right\}$$

and optimal approximation residual as

$$\psi^*(Y) = R(Y) - G^{*T} \phi(Y).$$

Then, we obtain $|\psi^*(Y)| \leq \psi$.

Definition 1 ([37]). *Given a continuous-time system*

$$\dot{X} = F(X), \tag{5}$$

where $X \in \mathbb{R}^n$ is the state vector and initial state is $X(t_0) = X_0$. Assume that there exists $\varpi > 0$ and $T(\varpi, X_0) < \infty$ such that $\|X(t)\| < \varpi$ for all X_0 and $t \geq t_0 + T(\varpi, X_0)$, and there is a constant $T_{max} > 0$ such that $T \leq T_{max}$ for any X_0. Then, the state is practically fixed-time stable.

Lemma 2 ([37]). *Suppose that there exists a Lyapunov function $V(X(t))$ for the system* (5) *such that*

$$\dot{V}(X(t)) \leq -aV^p(X(t)) - bV^q(X(t)) + c,$$

with constants $a > 0$, $b > 0$, $c > 0$, $0 < p < 1$, and $q > 1$. Then, $X(t)$ is practical fixed-time stable and converges to the set $\left\{ X(t) | \frac{1}{2} X^2(t) \leq V_m \right\}$ with $V_m = \min \left[\left(\frac{c}{a(1-\kappa)} \right)^{\frac{1}{p}}, \left(\frac{c}{b(1-\kappa)} \right)^{\frac{1}{q}} \right]$, where the settling time T is determined by $T \leq \bar{T} = \frac{1}{a\kappa(1-p)} + \frac{1}{b\kappa(q-1)}$ with $0 < \kappa < 1$.

Lemma 3 ([28]). *For any positive real numbers ς_i, ξ_i and a positive integer n, one has*

$$\sum_{i=1}^{n} \left(\varsigma_i^{\frac{3}{4}} + \xi_i^{\frac{3}{4}} \right) \geq \left[\sum_{i=1}^{n} (\varsigma_i + \xi_i) \right]^{\frac{3}{4}},$$
$$\sum_{i=1}^{n} \left(\varsigma_i^2 + \xi_i^2 \right) \geq \frac{1}{n} \left[\sum_{i=1}^{n} (\varsigma_i + \xi_i) \right]^2.$$

Lemma 4 ([38] Young's inequality). *For any positive real number ρ_a, ρ_b, ρ_c, and ρ_d satisfying $\frac{1}{\rho_a} + \frac{1}{\rho_b} = 1$, one has*

$$\rho_c \rho_d \leq \frac{\rho_c^{\rho_a}}{\rho_a} + \frac{\rho_d^{\rho_b}}{\rho_b}. \tag{6}$$

3. Problem Formulation

In this paper, the control objective is summarized as follows.

Control Objective: Given a bounded reference, the control objective is to propose a fixed-time tracking control approach for the strict-feedback nonlinear system (1) such that system output $Y(t)$ can track the reference signal $X_d(t)$ before $t \leq T_{max}$ with a constant T_{max}.

4. Fixed-Time Adaptive Controller Design with Novel DSC filters and Stability Analysis

In this section, a fixed-time adaptive controller with novel DSC filters is designed. The overall design can be shown in Figure 2.
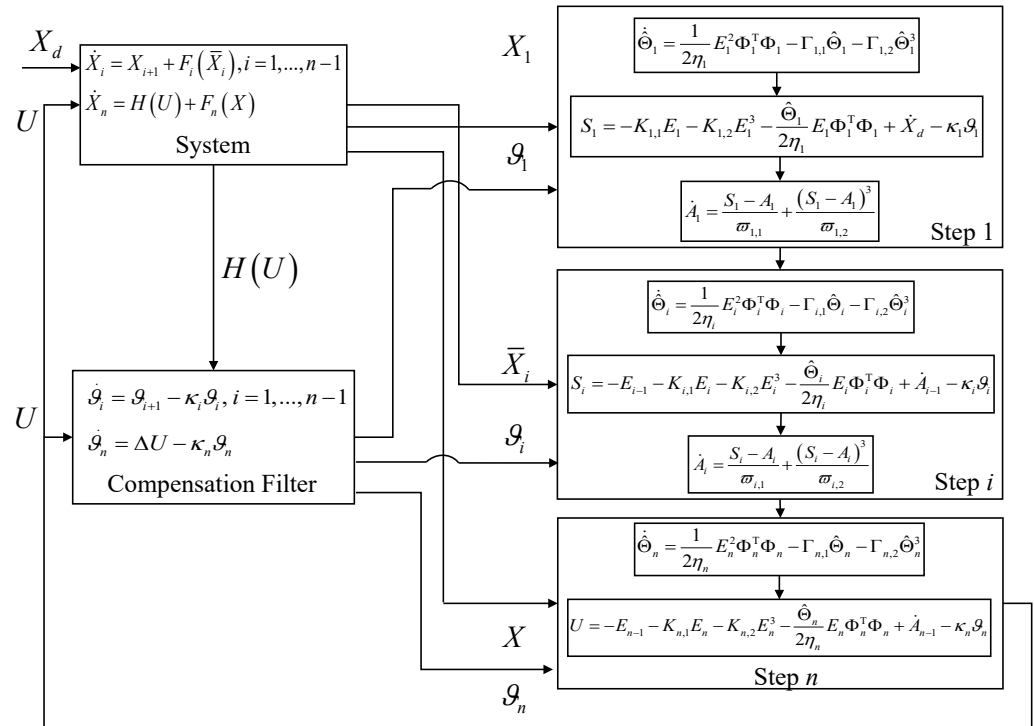
Figure 2. The flow chart of the presented design.

To tackle the input hysteresis, a compensation mechanism is introduced as

$$
\dot{\vartheta}_i = \vartheta_{i+1} - \kappa_i \vartheta_i, \ i = 1, \ldots, n-1,
$$
$$
\dot{\vartheta}_n = \Delta U - \kappa_n \vartheta_n, \tag{7}
$$

where $\Delta U = H(U) - U$ is the influence of the input hysteresis, $\kappa_i > 0$ is a constant, and the initial state is $\vartheta_i(0) = 0$. Define tracking errors E_i and filter errors Z_i as

$$
E_i = X_i - A_{i-1} - \vartheta_i, \ i = 1, \ldots, n,
$$
$$
Z_i = A_i - S_i, \ i = 1, \ldots, n-1, \tag{8}
$$

where S_i and A_i are designed later. In addition, we denote $A_0 = X_d$.

Using RBFNNs to estimate the unknown functions $F_i(\bar{X}_i)$ yields

$$
F_i(\bar{X}_i) = G_i^{*T} \Phi_i(\bar{X}_i) + \psi_i^*(\bar{X}_i). \tag{9}
$$

Due to the unknown optimal weight G_i^*, the adaptive parameter $\hat{\Theta}_i$ is defined as the estimation of Θ_i with $\Theta_i = \left\| G_i^* \right\|^2$. Furthermore, the parameter approximation error is denoted as $\tilde{\Theta}_i = \Theta_i - \hat{\Theta}_i$.

4.1. Adaptive Backstepping-Based Controller Design

4.1.1. Step 1

On account of (8), taking the time derivative of E_1 results in

$$
\dot{E}_1 = G_1^{*T} \Phi_1(X_1) + \psi_1^*(X_1) + E_2 + S_1 + Z_1 - \dot{X}_d + \kappa_1 \vartheta_1. \tag{10}
$$

The virtual control is designed as

$$S_1 = -K_{1,1}E_1 - K_{1,2}E_1^3 - \frac{\hat{\Theta}_1}{2\eta_1}E_1\Phi_1^T\Phi_1 + \dot{X}_d - \kappa_1\vartheta_1, \tag{11}$$

where $\eta_1 > 0$, $K_{1,1} > 0$, and $K_{1,2} > 0$ are constants. To avoid the differentiation of S_1, a novel DSC filter is developed as

$$\dot{A}_1 = \frac{S_1 - A_1}{\varpi_{1,1}} + \frac{(S_1 - A_1)^3}{\varpi_{1,2}}, \; A_1(0) = 0, \tag{12}$$

with constants $\varpi_{1,1} > 0$ and $\varpi_{1,2} > 0$. To resolve the parameter approximation problem, a fixed-time adaptive law is proposed as

$$\dot{\hat{\Theta}}_1 = \frac{1}{2\eta_1}E_1^2\Phi_1^T\Phi_1 - \Gamma_{1,1}\hat{\Theta}_1 - \Gamma_{1,2}\hat{\Theta}_1^3, \; \hat{\Theta}_1(0) \geq 0, \tag{13}$$

with constants $\Gamma_{1,1} > 0$ and $\Gamma_{1,2} > 0$.

4.1.2. Step $i(2 \leq i \leq n-1)$

From (8), taking the derivative of E_i leads to

$$\dot{E}_i = G_i^{*T}\Phi_i(\bar{X}_i) + \psi_i^*(\bar{X}_i) + E_{i+1} + S_i + Z_i - \dot{A}_{i-1} + \kappa_i\vartheta_i. \tag{14}$$

Design

$$S_i = -E_{i-1} - K_{i,1}E_i - K_{i,2}E_i^3 - \frac{\hat{\Theta}_i}{2\eta_i}E_i\Phi_i^T\Phi_i + \dot{A}_{i-1} - \kappa_i\vartheta_i, \tag{15}$$

with constants $\eta_i > 0$, $K_{i,1} > 0$, and $K_{i,2} > 0$. To avoid the differentiation of S_i, introduce a novel DSC filter as

$$\dot{A}_i = \frac{S_i - A_i}{\varpi_{i,1}} + \frac{(S_i - A_i)^3}{\varpi_{i,2}}, \; A_i(0) = 0, \tag{16}$$

where $\varpi_{i,1} > 0$ and $\varpi_{i,2} > 0$ are constants. To handle the parameter approximation problem, an adaptive law is developed as

$$\dot{\hat{\Theta}}_i = \frac{1}{2\eta_i}E_i^2\Phi_i^T\Phi_i - \Gamma_{i,1}\hat{\Theta}_i - \Gamma_{i,2}\hat{\Theta}_i^3, \; \hat{\Theta}_i(0) \geq 0, \tag{17}$$

with positive constants $\Gamma_{i,1}$ and $\Gamma_{i,2}$.

4.1.3. Step n

On the basis of (7) and (8), differentiating E_n yields

$$\begin{aligned}\dot{E}_n &= G_n^{*T}\Phi_n(X) + \psi_n^*(X) + H(U) - \dot{A}_{n-1} - \Delta U + \kappa_n\vartheta_n \\ &= G_n^{*T}\Phi_n(X) + \psi_n^*(X) + U - \dot{A}_{n-1} + \kappa_n\vartheta_n.\end{aligned} \tag{18}$$

Design

$$U = -E_{n-1} - K_{n,1}E_n - K_{n,2}E_n^3 - \frac{\hat{\Theta}_n}{2\eta_n}E_n\Phi_n^T\Phi_n + \dot{A}_{n-1} - \kappa_n\vartheta_n, \tag{19}$$

with $\eta_n > 0$, $K_{n,1} > 0$, and $K_{n,2} > 0$.

To approximate the adaptive parameter Θ_n, a fixed-time adaptive law is constructed as

$$\dot{\hat{\Theta}}_n = \frac{1}{2\eta_n} E_n^2 \Phi_n^{\mathrm{T}} \Phi_n - \Gamma_{n,1} \hat{\Theta}_n - \Gamma_{n,2} \hat{\Theta}_n^3, \ \hat{\Theta}_n(0) \geq 0, \tag{20}$$

where $\Gamma_{n,1}$ and $\Gamma_{n,2}$ are positive constants.

4.2. Stability Analysis

Next, to demonstrate the feasibility of the developed design in Section 4, the stability of the closed-loop system is analyzed.

4.2.1. Step 1

Substituting (11) into (10), one has

$$\dot{E}_1 = G_1^{*T} \Phi_1(X_1) + \psi_1^*(X_1) - K_{1,1} E_1 + Z_1 + E_2 - K_{1,2} E_1^3 - \frac{\hat{\Theta}_1}{2\eta_1} E_1 \Phi_1^{\mathrm{T}} \Phi_1. \tag{21}$$

The Lyapunov function for E_1 and $\tilde{\Theta}_1$ is chosen as

$$V_1\left(E_1, Z_1, \tilde{\Theta}_1\right) = \frac{1}{2} E_1^2 + \frac{1}{2} Z_1^2 + \frac{1}{2} \tilde{\Theta}_1^2. \tag{22}$$

Taking the derivative of V_1 results in

$$\begin{aligned}
\dot{V}_1 &= E_1 \dot{E}_1 + Z_1 \dot{Z}_1 - \tilde{\Theta}_1 \dot{\hat{\Theta}}_1 \\
&= E_1 G_1^{*T} \Phi_1(X_1) + E_1 \psi_1^*(Y_1) - K_{1,1} E_1^2 + E_1 E_2 + E_1 Z_1 \\
&\quad + Z_1 \dot{Z}_1 - K_{1,2} E_1^4 - \frac{\hat{\Theta}_1}{2\eta_1} E_1^2 \Phi_1^{\mathrm{T}} \Phi_1 - \tilde{\Theta}_1 \dot{\hat{\Theta}}_1.
\end{aligned} \tag{23}$$

Utilizing the Young's inquality yields

$$\begin{aligned}
E_1 G_1^{*T} \Phi_1(X_1) &\leq \frac{\Theta_1}{2\eta_1} E_1^2 \Phi_1^{\mathrm{T}} \Phi_1 + \frac{\eta_1}{2}, \\
E_1 \psi_1^*(X_1) &\leq |E_1| \psi_1 \leq \frac{1}{2}\left(E_1^2 + \psi_1^2\right).
\end{aligned} \tag{24}$$

Substituting (24) into (23), we obtain

$$\begin{aligned}
\dot{V}_1 &\leq -K_{1,1} E_1^2 - K_{1,2} E_1^4 + E_1 E_2 + E_1 Z_1 + \frac{E_1^2 + \psi_1^2}{2} \\
&\quad + Z_1 \dot{Z}_1 + \frac{\eta_1}{2} - \tilde{\Theta}_1 \left(\dot{\hat{\Theta}}_1 - \frac{1}{2\eta_1} E_1^2 \Phi_1^{\mathrm{T}} \Phi_1 \right).
\end{aligned} \tag{25}$$

Recalling the adaptive law (13), $\dot{V}_1$ becomes

$$\begin{aligned}
\dot{V}_1 &\leq -\left(K_{1,1} - \frac{1}{2} \right) E_1^2 - K_{1,2} E_{i,1}^4 + E_1 E_2 + E_1 Z_1 \\
&\quad + Z_1 \dot{Z}_1 + \frac{\psi_1^2}{2} + \frac{\eta_1}{2} + \Gamma_{1,1} \tilde{\Theta}_1 \hat{\Theta}_1 + \Gamma_{1,2} \tilde{\Theta}_1 \hat{\Theta}_1^3.
\end{aligned} \tag{26}$$

4.2.2. Step $i(2 \leq i \leq n-1)$

Inserting (15) into (14), one has

$$\dot{E}_i = G_i^{*T} \Phi_i(X_i) + \psi_i^*(\bar{X}_i) - E_{i-1} - K_{i,1} E_i + Z_i + E_{i+1} - K_{i,2} E_i^3 - \frac{\hat{\Theta}_i}{2\eta_i} E_i \Phi_i^{\mathrm{T}} \Phi_i. \tag{27}$$

Select Lyapunov function for E_i and $\tilde{\Theta}_i$ as

$$V_i(E_i, Z_i, \tilde{\Theta}_i) = \frac{1}{2}E_i^2 + \frac{1}{2}Z_i^2 + \frac{1}{2}\tilde{\Theta}_i^2. \tag{28}$$

Differentiating V_i, one has

$$\begin{aligned}
\dot{V}_i &= E_i\dot{E}_i + Z_i\dot{Z}_i - \tilde{\Theta}_i\dot{\hat{\Theta}}_i \\
&= E_i G_i^{*T}\Phi_i(\bar{X}_i) + E_i\psi_i^*(\bar{X}_i) - K_{i,1}E_i^2 - K_{i,2}E_i^4 \\
&\quad + Z_i\dot{Z}_i - E_{i-1}E_i + E_iE_{i+1} - \frac{\hat{\Theta}_i}{2\eta_i}E_i^2\Phi_i^T\Phi_i - \tilde{\Theta}_i\dot{\hat{\Theta}}_i.
\end{aligned} \tag{29}$$

Recalling the Young's inequality, we have

$$E_i G_i^{*T}\Phi_i(\bar{X}_i) \leq \frac{\Theta_i}{2\eta_i}E_i^2\Phi_i^T\Phi_i + \frac{\eta_i}{2},$$

$$E_i\psi_i^*(\bar{X}_i) \leq |E_i|\psi_i \leq \frac{1}{2}\left(E_i^2 + \psi_i^2\right). \tag{30}$$

Inserting (30) into (29) leads to

$$\begin{aligned}
\dot{V}_i \leq{}& -K_{i,1}E_i^2 - K_{i,2}E_i^4 - E_{i-1}E_i + E_iE_{i+1} + E_iZ_i + \frac{\eta_i}{2} \\
&+ Z_i\dot{Z}_i + \frac{E_i^2 + \psi_i^2}{2} - \tilde{\Theta}_i\left(\dot{\hat{\Theta}}_i - \frac{1}{2\eta_i}E_i^2\Phi_i^T\Phi_i\right).
\end{aligned} \tag{31}$$

On the basis of the fixed-time adaptive law (17), $\dot{V}_i$ becomes

$$\begin{aligned}
\dot{V}_i \leq{}& -\left(K_{i,1} - \frac{1}{2}\right)E_i^2 - K_{i,2}E_{i,1}^4 - E_{i-1}E_i + E_iE_{i+1} \\
&+ E_iZ_i + Z_i\dot{Z}_i + \frac{\psi_i^2}{2} + \frac{\eta_i}{2} + \Gamma_{i,1}\tilde{\Theta}_i\hat{\Theta}_i + \Gamma_{i,2}\tilde{\Theta}_i\hat{\Theta}_i^3.
\end{aligned} \tag{32}$$

4.2.3. Step n

Inserting (19) into (18), we obtain

$$\dot{E}_n = G_n^{*T}\Phi_n(X) + \psi_n^*(X) - E_{n-1} - K_{n,1}E_n - K_{n,2}E_n^3 - \frac{\hat{\Theta}_n}{2\eta_n}E_n\Phi_n^T\Phi_n. \tag{33}$$

The Lyapunov function for E_n and $\tilde{\Theta}_n$ is chosen as

$$V_n(E_n, \tilde{\Theta}_n) = \frac{1}{2}E_n^2 + \frac{1}{2}\tilde{\Theta}_n^2. \tag{34}$$

The derivative of V_n satisfies

$$\begin{aligned}
\dot{V}_n &= E_n\dot{E}_n - \tilde{\Theta}_n\dot{\hat{\Theta}}_n \\
&= E_n G_n^{*T}\Phi_n(X) + E_n\psi_n^*(X) - K_{n,1}E_n^2 - K_{n,2}E_n^4 \\
&\quad - E_{n-1}E_n - \frac{\hat{\Theta}_n}{2\eta_n}E_n^2\Phi_n^T\Phi_n - \tilde{\Theta}_n\dot{\hat{\Theta}}_n.
\end{aligned} \tag{35}$$

Using the Young's inquality, one obtains

$$E_n G_n^{*T}\Phi_n(X) \leq \frac{\Theta_n}{2\eta_n}E_n^2\Phi_n^T\Phi_n + \frac{\eta_n}{2},$$

$$E_n\psi_n^*(X) \leq |E_n|\psi_n \leq \frac{1}{2}\left(E_n^2 + \psi_n^2\right). \tag{36}$$

Substituting (36) into (35), one has

$$
\dot{V}_n \le -K_{n,1}E_n^2 - K_{n,2}E_n^4 - E_{n-1}E_n + \frac{\eta_n}{2}
$$
$$
+ \frac{E_n^2 + \psi_n^2}{2} - \tilde{\Theta}_n\left(\dot{\hat{\Theta}}_n - \frac{1}{2\eta_n}E_n^2\Phi_n^T\Phi_n\right). \tag{37}
$$

From (20), $\dot{V}_n$ is transformed as

$$
\dot{V}_n \le -\left(K_{n,1} - \frac{1}{2}\right)E_n^2 - K_{n,2}E_n^4 - E_{n-1}E_n
$$
$$
+ \frac{\psi_n^2}{2} + \frac{\eta_n}{2} + \Gamma_{n,1}\tilde{\Theta}_n\hat{\Theta}_n + \Gamma_{n,2}\tilde{\Theta}_n\hat{\Theta}_n^3. \tag{38}
$$

Theorem 1. *For the strict-feedback nonlinear system (1) with the developed design in Section 4, there exists $T_m > 0$ such that the fixed-time performance can be obtained with settling time $T \le T_m$.*

Proof. The Lyapunov function is defined as

$$
V = \sum_{i=1}^{n} V_i.
$$

The first-order derivative of V satisfies

$$
\dot{V} \le -\sum_{i=1}^{n}\left(K'_{i,1}E_i^2 + K_{i,2}E_i^4\right) + \frac{1}{2}\sum_{i=1}^{n}\left(\psi_i^2 + \eta_i\right)
$$
$$
+ \sum_{i=1}^{n-1}\left(E_iZ_i + Z_i\dot{Z}_i\right) + \sum_{i=1}^{n}\left[\Gamma_{i,1}\tilde{\Theta}_i\hat{\Theta}_i + \Gamma_{i,2}\tilde{\Theta}_i\hat{\Theta}_i^3\right], \tag{39}
$$

with $k'_{i,1} = K_{i,1} - \frac{1}{2}$.

The derivative of Z_i is

$$
\dot{Z}_i = \dot{A}_i - \dot{S}_i = -\frac{Z_i}{\varpi_{i,1}} - \frac{Z_i^3}{\varpi_{i,2}} - \dot{S}_i,
$$

where

$$
\dot{S}_1 = -K_{1,1}\dot{E}_1 - 3K_{1,2}E_1^2\dot{E}_1 - \kappa_1\dot{\vartheta}_1 + \ddot{X}_d - \frac{\dot{\hat{\Theta}}_1}{2\eta_1}E_1\Phi_1^T\Phi_1 - \frac{\hat{\Theta}_1}{2\eta_1}\dot{E}_1\Phi_1^T\Phi_1 - \frac{\hat{\Theta}_1}{\eta_1}E_1\Phi_1^T\dot{\Phi}_1
$$

and

$$
\dot{S}_i = -\dot{E}_{i-1} - K_{i,1}\dot{E}_i - 3K_{i,2}E_i^2\dot{E}_i - \kappa_i\dot{\vartheta}_i - \frac{\dot{Z}_{i-1}}{\varpi_{i-1,1}} - \frac{3Z_{i-1}^2\dot{Z}_{i-1}}{\varpi_{i-1,2}}
$$
$$
- \frac{\dot{\hat{\Theta}}_i}{2\eta_i}E_i\Phi_i^T\Phi_i - \frac{\hat{\Theta}_i}{2\eta_i}\dot{E}_i\Phi_i^T\Phi_i - \frac{\hat{\Theta}_i}{\eta_i}E_i\Phi_i^T\dot{\Phi}_i, i = 2,\ldots,n-1
$$

are continuous on Ω_i, where

$$
\Omega_i = \left\{(E_i, Z_i, \vartheta_i)\,\middle|\, E_i^2 + Z_i^2 + \vartheta_i^2 \le R_i\right\},
$$

and $R_0 > 0$ and $R_i > 0$ [20]. Therefore, $|\dot{S}_i| \leq M_i$ with $M_i > 0$. Employing the Young's inequality, one obtains

$$
\begin{aligned}
E_i Z_i &\leq \frac{E_i^2}{2} + \frac{Z_i^2}{2}, \\
Z_i \dot{Z}_i &\leq \frac{\eta_0 Z_i^2}{2} + \frac{M_i^2}{2\eta_0}.
\end{aligned}
\tag{40}
$$

From Lemma 3, the following inequalities hold

$$
\begin{aligned}
\left(E_i^2\right)^{\frac{3}{4}} &\leq \frac{3}{4}\left(E_i^2\right) + \frac{1}{4}, \\
\left(\tilde{\Theta}_i^2\right)^{\frac{3}{4}} &\leq \frac{3}{4}\left(\tilde{\Theta}_i^2\right) + \frac{1}{4}.
\end{aligned}
\tag{41}
$$

From Young's inequality, we have

$$
\begin{aligned}
\tilde{\Theta}_i \hat{\Theta}_i &\leq \frac{1}{2}\Theta_i^2 - \frac{1}{2}\tilde{\Theta}_i^2 \leq \frac{1}{2}\Theta_i^2 + \frac{1}{6} - \frac{2}{3}\left(\tilde{\Theta}_i^2\right)^{\frac{3}{4}} \\
\tilde{\Theta}_i \hat{\Theta}_i^3 &= \tilde{\Theta}_i \Theta_i^3 - \Theta_i^2 \tilde{\Theta}_i^2 + \Theta_i \tilde{\Theta}_i^3 - \tilde{\Theta}_i^4 \\
&\leq \Gamma_{i,3}\frac{\tilde{\Theta}_i^4}{4} + \Gamma_{i,3}^{\frac{1}{3}}\frac{3\Theta_i^4}{4} + \frac{\Theta_i^4}{2\Gamma_{i,3}} + \Gamma_{i,3}\frac{\tilde{\Theta}_i^4}{2} \\
&\quad + \Gamma_{i,4}^{\frac{1}{3}}\frac{3\tilde{\Theta}_i^4}{4} + \Gamma_{i,4}\frac{\Theta_i^4}{4} - \tilde{\Theta}_i^4 \\
&= -\left(1 - \frac{3}{4}\left(\Gamma_{i,3} + \Gamma_{i,4}^{\frac{1}{3}}\right)\right)\tilde{\Theta}_i^4 \\
&\quad + \left(\frac{3}{4}\Gamma_{i,3}^{\frac{1}{3}} + \frac{1}{2\Gamma_{i,3}} + \frac{1}{4}\Gamma_{i,4}\right)\Theta_i^4,
\end{aligned}
\tag{42}
$$

with $\Gamma_{i,3} > 0, \Gamma_{i,4} > 0, 1 - \frac{3}{4}\left(\Gamma_{i,3} + \Gamma_{i,4}^{\frac{1}{3}}\right) > 0$. Due to Lemma 3, one has

$$
\begin{aligned}
\sum_{j=1}^{n}\left[\left(E_i^2\right)^{\frac{3}{4}} + \left(\tilde{\Theta}_i^2\right)^{\frac{3}{4}}\right] &\geq \left[\sum_{j=1}^{n}\left(E_i^2 + \tilde{\Theta}_i^2\right)\right]^{\frac{3}{4}}, \\
\sum_{j=1}^{n}\left[\left(E_i^2\right)^2 + \left(\tilde{\Theta}_i^2\right)^2\right] &\geq \frac{1}{n}\left[\sum_{j=1}^{n}\left(E_i^2 + \tilde{\Theta}_i^2\right)\right]^2.
\end{aligned}
\tag{43}
$$

Inserting (40)–(43) into (39) obtains

$$
\begin{aligned}
\dot{V} &\leq -\sum_{i=1}^{n}\left[\frac{4}{3}K'_{i,1}\left(E_i^2\right)^{\frac{3}{4}} + \frac{2\Gamma_{i,1}}{3}\left(\tilde{\Theta}_i^2\right)^{\frac{3}{4}}\right] + \frac{1}{2}\sum_{i=1}^{n}\left(\psi_i^2 + \eta_i\right) + \frac{1}{6}\sum_{i=1}^{n}\left(2K'_{i,1} + \Gamma_{i,1}\right) \\
&\quad - \sum_{i=1}^{n}\frac{\Gamma_{i,2}}{4}\left(4 - 3\Gamma_{i,3} - 3\Gamma_{i,4}^{\frac{1}{3}}\right)\tilde{\Theta}_i^4 - \sum_{i=1}^{n}K_{i,2}E_i^4 + \frac{1}{2}\sum_{i=1}^{n}\Gamma_{i,1}\Theta_i^2 \\
&\quad + \frac{1}{2}\sum_{i=1}^{n}\Gamma_{i,2}\left(\frac{3}{2}\Gamma_{i,3}^{\frac{1}{3}} + \frac{1}{\Gamma_{i,3}} + \frac{1}{2}\Gamma_{i,4}\right)\Theta_i^4 \\
&\leq -a_1 V^{\frac{3}{4}} - \frac{a_2}{n}V^2 + b,
\end{aligned}
\tag{44}
$$

with

$$a_1 = 2^{\frac{3}{4}} \min_{i=1,\ldots,n} \left\{ \frac{4K'_{i,1}}{3}, \frac{2\Gamma_{i,1}}{3} \right\},$$

$$a_2 = 4 \min_{i=1,\ldots,n} \left\{ K_{i,2}, \frac{\Gamma_{i,2}}{4} \left(4 - 3\Gamma_{i,3} - 3\Gamma_{i,4}^{\frac{1}{3}} \right) \right\},$$

$$b = \frac{1}{2} \sum_{i=1}^{n} \left(\Gamma_{i,1}\Theta_i^2 + \psi_i^2 + \eta_i \right) + \frac{1}{6} \sum_{i=1}^{n} \left(2K'_{i,1} + \Gamma_{i,1} \right)$$

$$+ \frac{1}{2} \sum_{i=1}^{n} \Gamma_{i,2} \left(\frac{3}{2}\Gamma_{i,3}^{\frac{1}{3}} + \frac{1}{\Gamma_{i,3}} + \frac{1}{2}\Gamma_{i,4} \right) \Theta_i^4.$$

On the basis of Lemma 2, E_i and $\tilde{\Theta}_i$ converge to

$$\left\{ (E_1, \tilde{\Theta}_1, \ldots, E_n, \tilde{\Theta}_n) | \frac{1}{2} \sum_{i=1}^{n} \left(E_i^2 + \tilde{\Theta}_i^2 \right) \leq V_s \right\}$$

before $t \leq T_{\max}$ with

$$T_{\max} = \max \left\{ \frac{4}{a_1 o} + \frac{1}{a_2}, \frac{4}{a_1} + \frac{1}{a_2 o} \right\},$$

$0 < o < 1$, and

$$V_s = \min \left\{ \left(\frac{b}{(1-o)a_1} \right)^{\frac{4}{3}}, \left(\frac{b}{(1-o)a_2} \right)^{\frac{1}{2}} \right\}.$$

As a consequence, based on the error definition (8), fixed-time convergence of E_i is proved. On the basis of the DSC filter design (12) and (16), $\dot{A}_i$ is bounded. Due to (7), (11), (15), and (19), S_i, U, A_i, and ϑ_i are bounded. According to (1) and (2), X_i and $H(U)$ are bounded. Finally, the fixed-time performance can be proved. $\square$

5. Simulation Results

5.1. Example 1

Consider the following system

$$\begin{aligned} \dot{X}_1 &= X_2 - X_1^2 \\ \dot{X}_2 &= X_3 + 2X_1X_2 \\ \dot{X}_3 &= H(U) + X_1X_3 - 2X_2X_3 + 5X_1X_2X_3 \\ Y &= X_1 \end{aligned}$$

with $X_d = 0.5[\sin(t) + \sin(2t)]$.

From the definition of $T_{\max}$ and V_S, to accelerate convergence speed, $T_{\max}$ and V_S should be reduced small enough, which requires enough large a_1 and a_2 and enough small b. On the basis of (44), to increase a_1 and a_2 and decrease b, we need to increase $K_{i,2}$ and decrease $\Gamma_{i,4}$, where $K_{i,1}$, $\Gamma_{i,1}$, $\Gamma_{i,2}$, and $\Gamma_{i,3}$ should be chosen neither too large nor too small.

We select the initial conditions as $X_1(0) = 0.2$, $X_2(0) = -2.5$, and $X_3(0) = -0.2$ and the design parameters as $K_{1,1} = 20$, $K_{2,1} = 210$, $K_{3,1} = 330$, $K_{1,2} = K_{2,2} = K_{3,2} = 2$, $\kappa_1 = \kappa_2 = \kappa_3 = 50$, $\varpi_{1,1} = \varpi_{2,1} = 0.1$, $\varpi_{1,2} = \varpi_{2,2} = 10$, $\Gamma_{1,1} = \Gamma_{2,1} = \Gamma_{3,1} = 5$, $\Gamma_{1,2} = 10$, $\Gamma_{2,2} = 20$, $\Gamma_{3,2} = 30$, and $\eta_1 = \eta_2 = \eta_3 = 0.5$.

The RBFNNs are selected as in (4), i.e., RBFNN $\Phi_1(X_1)$ contains three hidden nodes with the center distributing in $[-2, 0, 2]$. RBFNN $\Phi_2(\bar{X}_2)$ has 9 nodes with the center selected as $[-2, 0, 2] \times [-2, 0, 2]$. RBFNN $\Phi_3(X_3)$ contains 27 nodes, where the centers are chosen as $[-2, 0, 2] \times [-2, 0, 2] \times [-2, 0, 2]$.

The simulation results are shown in Figures 3–5. From Figure 3, one can observe the output converges to the reference. In Figure 4, the curves of filter errors and tracking errors are depicted. From Figure 5, the control input and the hysteresis nonlinearity are displayed.
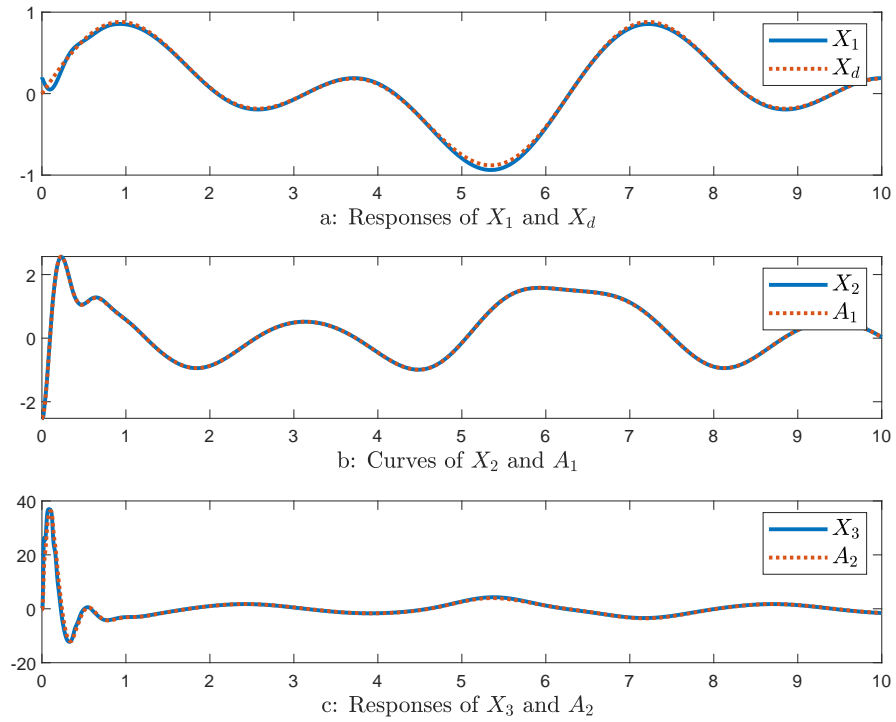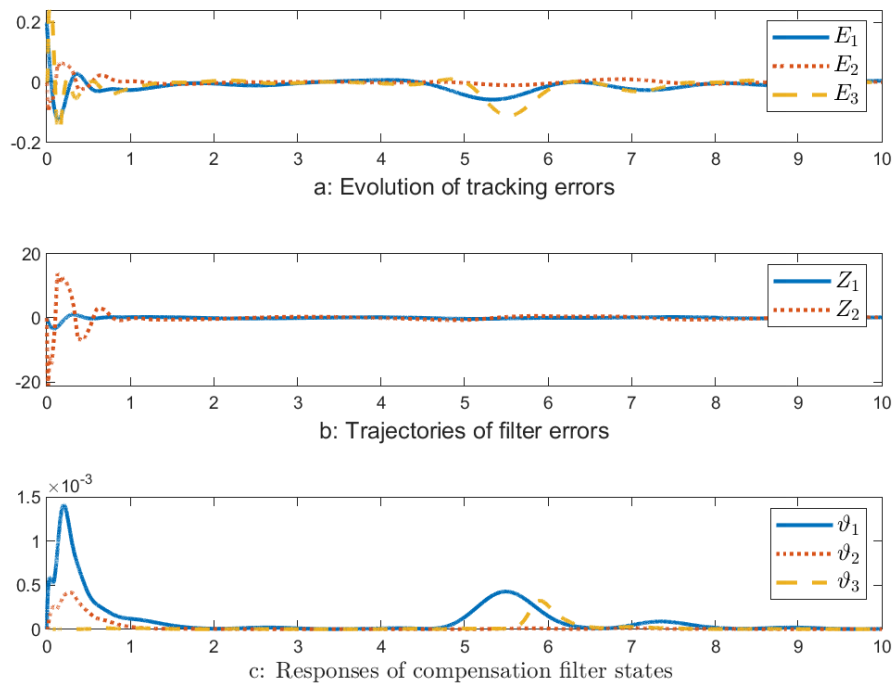
Figure 3. Output tracking performance.

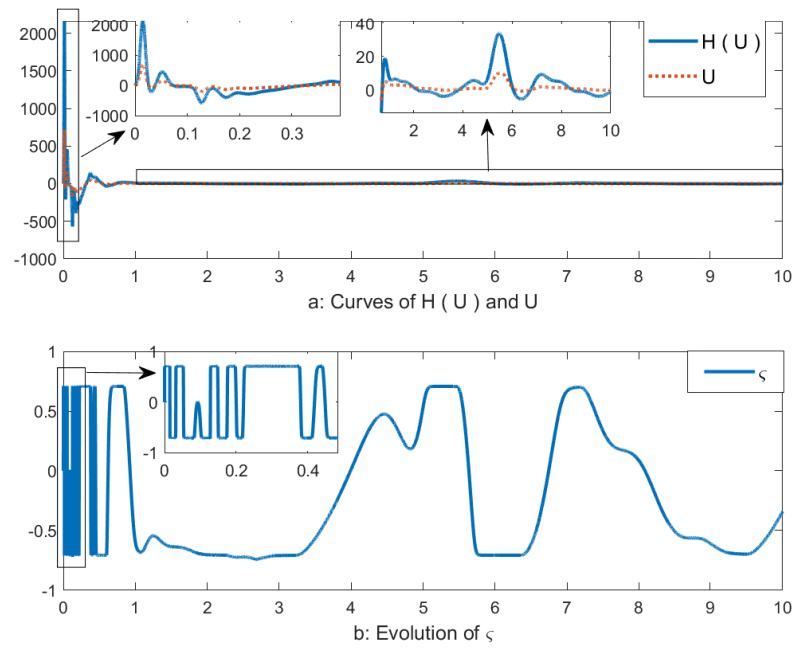**Figure 4.** Curves of error signals and compensation filter states.

Figure 5. The control input and hysteresis nonlinearity.

5.2. Example 2: Circuit System

This section provides a comparison between the approach in this paper with classic DSC-based methods [39] using a circuit system, where the circuit diagram is shown in Figure 6.
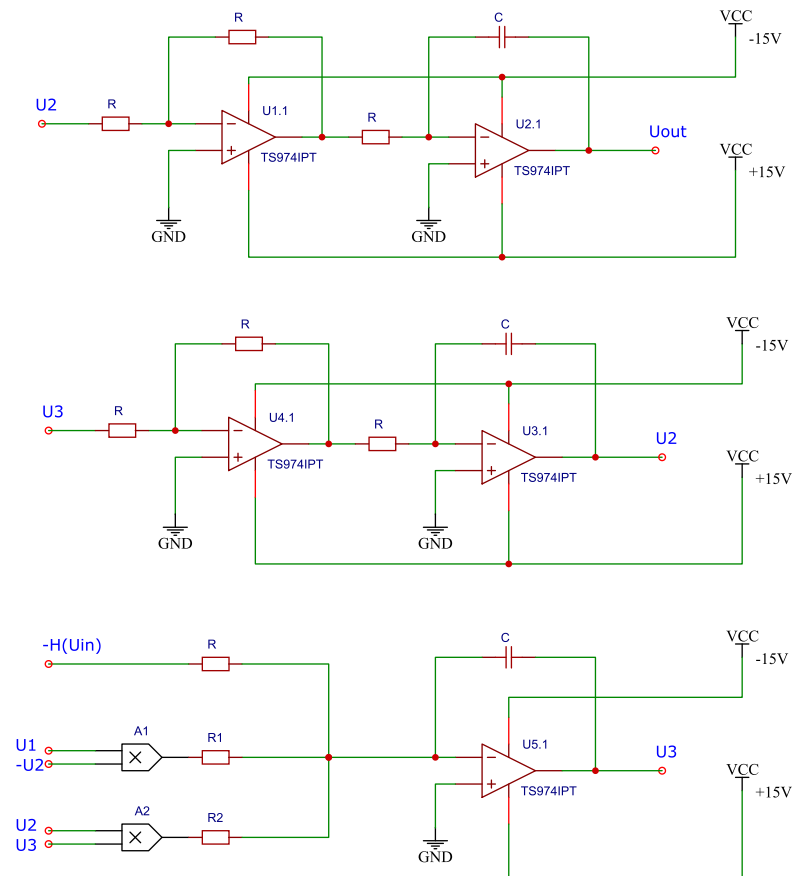

Figure 6. Circuit diagram.

The parameters are chosen as

$$R = 50\,\mathrm{k\Omega}, C = 20\,\mathrm{pF}, R1 = 250\,\mathrm{k\Omega}, R2 = 125\,\mathrm{k\Omega}$$

The circuit system can be modeled as

$$\begin{aligned}
\dot{X}_1 &= X_2 \\
\dot{X}_2 &= X_3 \\
\dot{X}_3 &= H(U) + 0.2X_1X_2 - 0.4X_2X_3 \\
Y &= X_1
\end{aligned}$$

with

$$X_1 = U_1, X_2 = U_2, X_3 = U_3, Y = Uout, U = Uin$$
$$X_d = 0.5[\sin(t) + \sin(2t)] \tag{45}$$

and initial conditions $X_1(0) = 0.3$, $X_2(0) = -1.5$, and $X_3(0) = -0.3$. For the design parameters, we select $K_{1,1} = 10$, $K_{2,1} = 150$, $K_{3,1} = 280$, $K_{1,2} = K_{2,2} = K_{3,2} = 1.5$, $\kappa_1 = \kappa_2 = \kappa_3 = 40$, $\varpi_{1,1} = \varpi_{2,1} = 0.1$, $\varpi_{1,2} = \varpi_{2,2} = 10$, $\Gamma_{1,1} = 6$, $\Gamma_{2,1} = 8$, $\Gamma_{3,1} = 7$, $\Gamma_{1,2} = 10$, $\Gamma_{2,2} = 20$, $\Gamma_{3,2} = 30$, and $\eta_1 = \eta_2 = \eta_3 = 0.5$.

The RBFNNs are selected the same as in Example 1, i.e., RBFNN $\Phi_1(X_1)$ contains three hidden nodes with the centers distributing in $[-2, 0, 2]$. RBFNN $\Phi_2(\bar{X}_2)$ has 9 nodes with the centers distributed in $[-2, 0, 2] \times [-2, 0, 2]$. RBFNN $\Phi_3(X_3)$ contains 27 nodes, where the centers are distributed in $[-2, 0, 2] \times [-2, 0, 2] \times [-2, 0, 2]$.

The simulation results of the method in this paper are shown in Figures 7–9. In Figure 7, the evolution of system states is displayed, where all system states converge to the reference signals. Figure 8 depicts the trajectories of filter errors and tracking errors. The control input and the hysteresis nonlinearity are displayed in Figure 9.
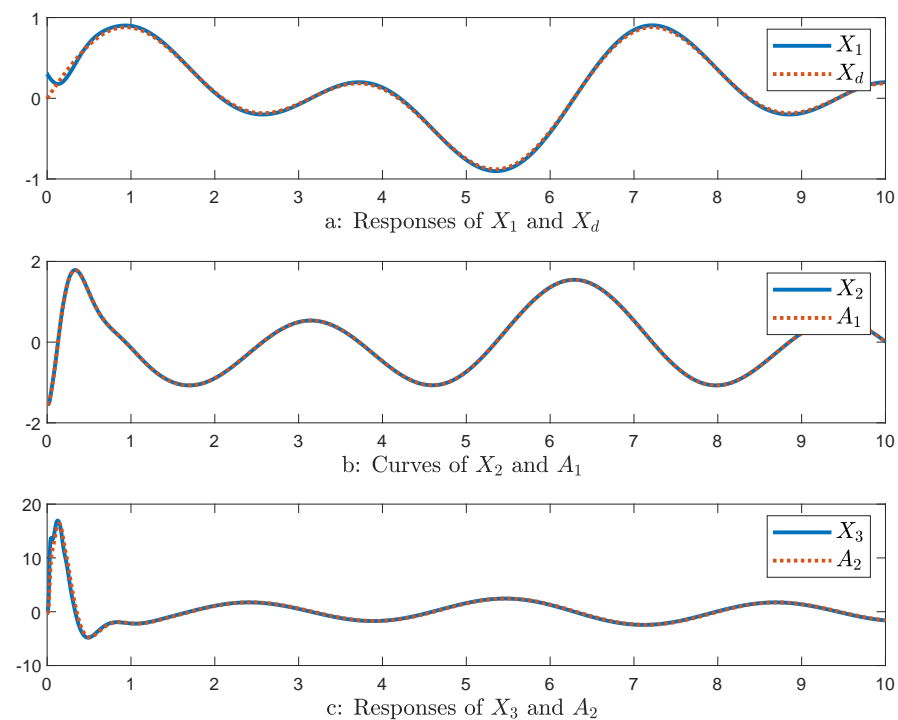

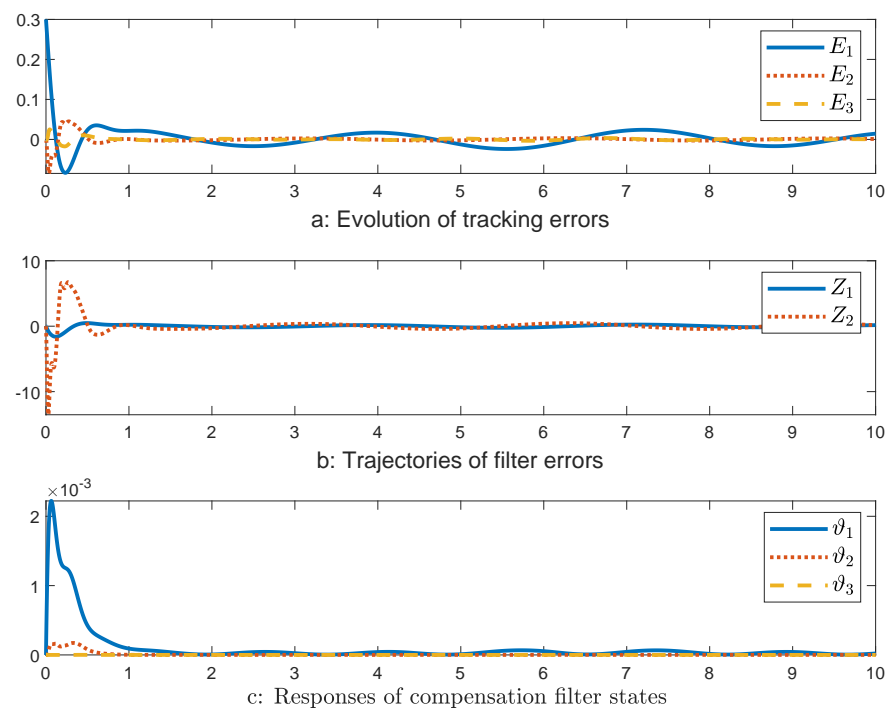**Figure 7.** Output tracking performance.

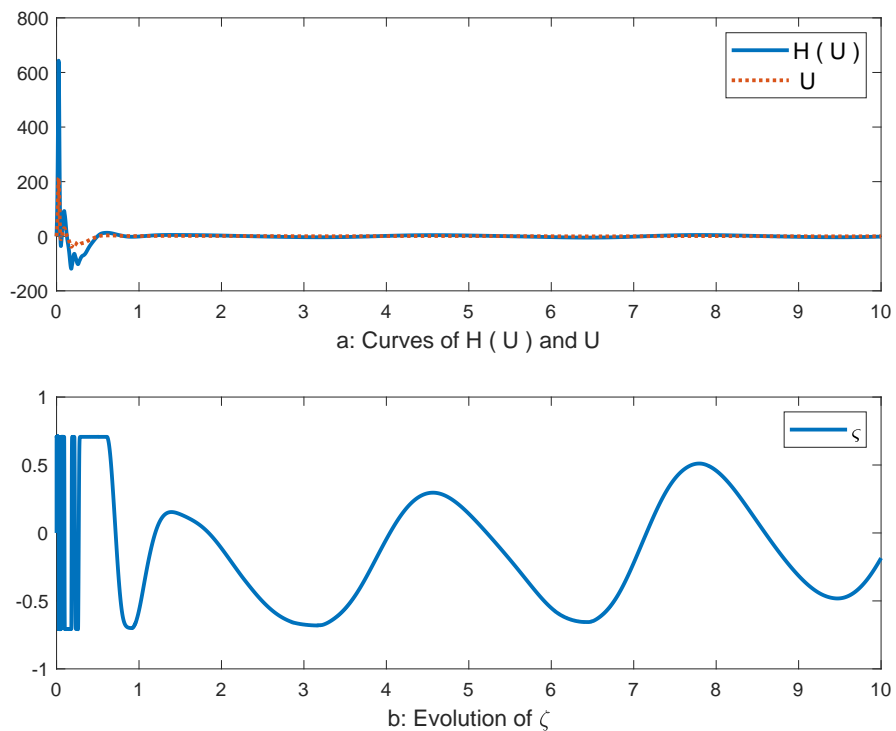**Figure 8.** Curves of error signals and compensation filter states.

Figure 9. The control input and hysteresis nonlinearity.

Utilizing the scheme in [39], the results are shown in Figures 10–12, where the presented method outperforms the method in [39]. In Figure 8, filter errors and tracking errors do not converge to zero. The control input and the hysteresis nonlinearity are given in Figure 9.
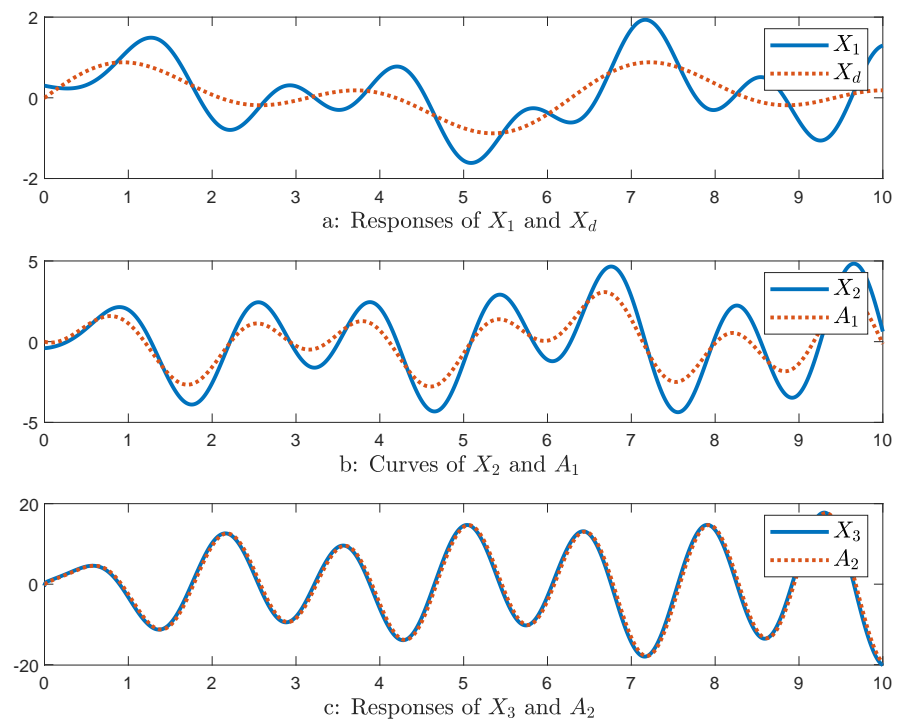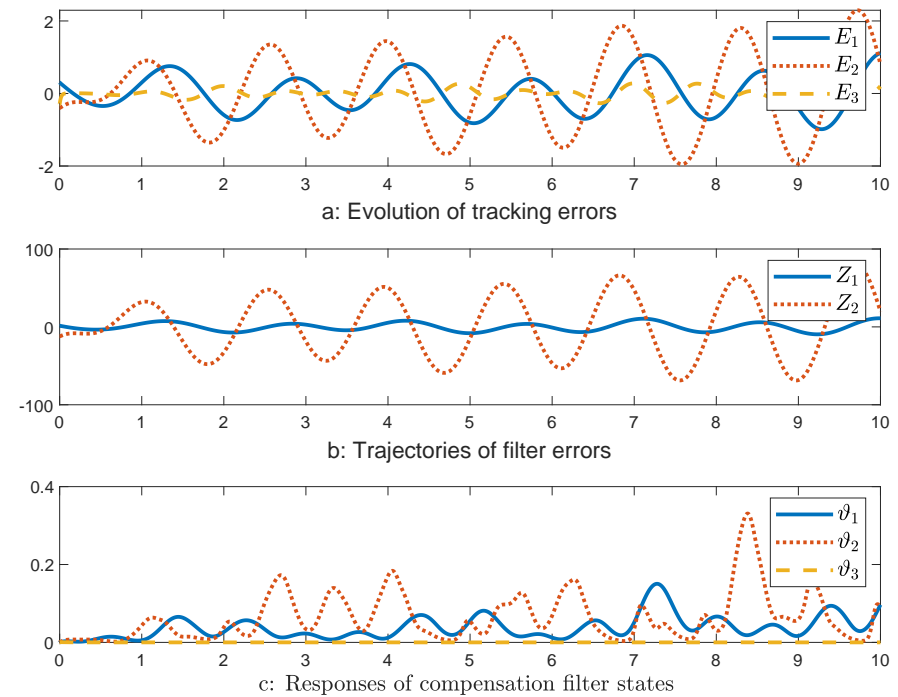
Figure 10. Output tracking performance.

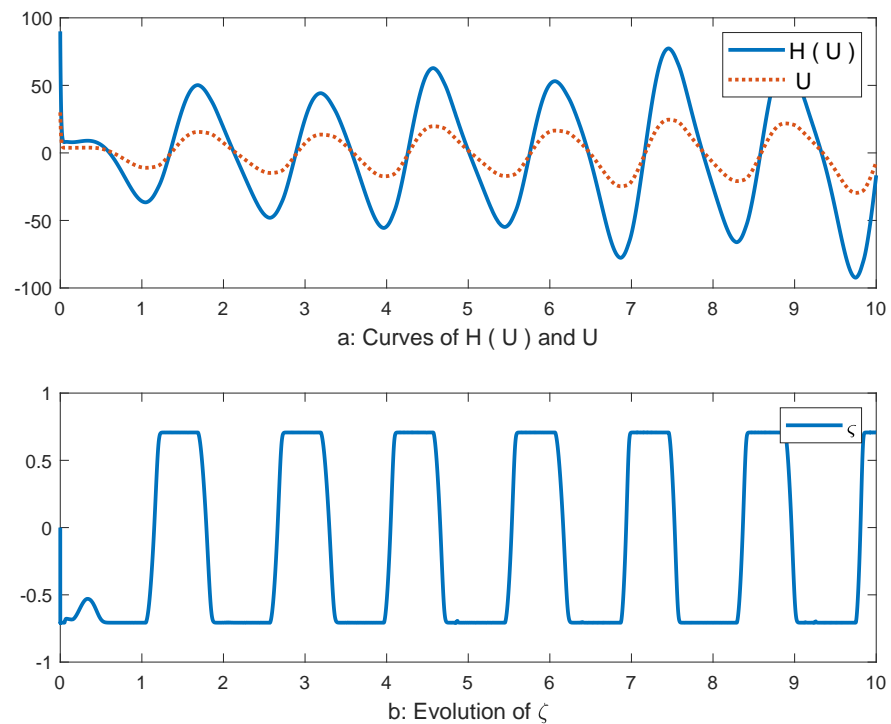**Figure 11.** Curves of error signals and compensation filter states.

Figure 12. The control input and hysteresis nonlinearity.

Based on the definition of $T_{\max}$, $T_{\max}$ is calculated as 0.83 s in Example 1 and 0.76 s in Example 2. From these figures, we can observe that the system states all converge to corresponding reference signals before $t = T_{\max}$, both in Examples 1 and 2. Therefore, the system states achieve fixed-time convergence indeed. It can be concluded that despite the input hysteresis, the method developed in this paper is verified as effective for the system (1).

6. Conclusions

In this paper, for strict-feedback systems with the input hysteresis, an adaptive tracking control approach is presented, where fixed-time convergence is achieved. The introduced compensation filter can overcome the effect of the input hysteresis. The constructed fixed-time adaptive law can ensure fixed-time properties of the parameter approximation errors. The novel DSC employed can tackle the explosion of complexity with the guarantee of fixed-time convergence. Moreover, singularity problems in the control input are excluded. Simulation results validate the effectiveness of the scheme proposed. Future works will extend the method presented to stochastic systems and dynamic uncertainties.

Author Contributions: Conceptualization, X.F. and J.C.; methodology, T.N.; software, X.F.; validation, X.F., J.C. and T.N.; formal analysis, J.C.; writing—original draft preparation, X.F.; writing—review and editing, T.N. All authors have read and agreed to the published version of the manuscript.

Conflicts of Interest: The authors declare no conflict of interest.

References

1. Alattas, K.A.; Mobayen, S.; Din, S.U.; Asad, J.H.; Fekih, A.; Assawinchaichote, W.; Vu, M.T. Design of a Non-Singular Adaptive Integral-Type Finite Time Tracking Control for Nonlinear Systems With External Disturbances. *IEEE Access* **2021**, *9*, 102091–102103. [CrossRef]
2. Mofid, O.; Amirkhani, S.; ud Din, S.; Mobayen, S.; Vu, M.T.; Assawinchaichote, W. Finite-time convergence of perturbed nonlinear systems using adaptive barrier-function nonsingular sliding mode control with experimental validation. *J. Vib. Control* **2022**. [CrossRef]
3. Dastres, H.; Rezaie, B.; Baigzadehnoe, B. Neural-network-based adaptive backstepping control for a class of unknown nonlinear time-delay systems with unknown input saturation. *Neurocomputing* **2020**, *398*, 131–152.
4. Kchaou, M.; Gassara, H.; El-Hajjaji, A. Adaptive sliding mode control for fuzzy singular systems with time delay and input nonlinearity. *Int. J. Adapt. Control Signal Process.* **2018**, *32*, 464–479.
5. Thanh, H.L.N.N.; Vu, M.T.; Mung, N.X.; Nguyen, N.P.; Phuong, N.T. Perturbation Observer-Based Robust Control Using a Multiple Sliding Surfaces for Nonlinear Systems with Influences of Matched and Unmatched Uncertainties. *Mathematics* **2020**, *8*, 1371.
6. Alattas, K.A.; Vu, M.T.; Mofid, O.; El-Sousy, F.F.M.; Alanazi, A.K.; Awrejcewicz, J.; Mobayen, S. Adaptive Nonsingular Terminal Sliding Mode Control for Performance Improvement of Perturbed Nonlinear Systems. *Mathematics* **2022**, *10*, 1064. [CrossRef]
7. Yang, Y.; Gao, W.; Modares, H.; Xu, C.Z. Robust Actor–Critic Learning for Continuous-Time Nonlinear Systems With Unmodeled Dynamics. *IEEE Trans. Fuzzy Syst.* **2022**, *30*, 2101–2112. [CrossRef]
8. Yang, Y.; Vamvoudakis, K.G.; Modares, H.; Yin, Y.; Wunsch, D.C. Hamiltonian-Driven Hybrid Adaptive Dynamic Programming. *IEEE Trans. Syst. Man, Cybern. Syst.* **2021**, *51*, 6423–6434. [CrossRef]
9. Yang, Y.; Modares, H.; Vamvoudakis, K.G.; He, W.; Xu, C.Z.; Wunsch, D.C. Hamiltonian-Driven Adaptive Dynamic Programming With Approximation Errors. *IEEE Trans. Cybern.* 2021, *early access*. [CrossRef]
10. Ghaffari, V.; Mobayen, S.; ud Din, S.; Rojsiraphisal, T.; Vu, M.T. Robust tracking composite nonlinear feedback controller design for time-delay uncertain systems in the presence of input saturation. *ISA Trans.* 2022, *in press*.
11. Yang, Y.; Tang, L.; Zou, W.; Guo, J.; Ahn, C.K. Dynamic Event-Triggered Design with Fixed-Time Performance and Input Dead-Zone. *IEEE Trans. Circuits Syst. II Express Briefs* 2022, *early access*. [CrossRef]
12. Li, H.; Huang, C.G.; Guedes Soares, C. A real-time inspection and opportunistic maintenance strategies for floating offshore wind turbines. *Ocean Eng.* **2022**, *256*, 111433. [CrossRef]
13. Li, H.; Díaz, H.; Guedes Soares, C. A failure analysis of floating offshore wind turbines using AHP-FMEA methodology. *Ocean Eng.* **2021**, *234*, 109261. [CrossRef]
14. Li, H.; Guedes Soares, C.; Huang, H.Z. Reliability analysis of a floating offshore wind turbine using Bayesian Networks. *Ocean Eng.* **2020**, *217*, 107827.
15. Zheng, X.; Yang, X. Improved adaptive NN backstepping control design for a perturbed PVTOL aircraft. *Neurocomputing* **2020**, *410*, 51–60.
16. Yang, Y.; Modares, H.; Vamvoudakis, K.G.; Yin, Y.; Wunsch, D.C. Dynamic Intermittent Feedback Design for H_∞ Containment Control on a Directed Graph. *IEEE Trans. Cybern.* **2020**, *50*, 3752–3765.
17. Zou, W.; Shi, P.; Xiang, Z.; Shi, Y. Finite-Time Consensus of Second-Order Switched Nonlinear Multi-Agent Systems. *IEEE Trans. Neural Netw. Learn. Syst.* **2020**, *31*, 1757–1762. [CrossRef]
18. Yang, Y.; Xu, C.Z. Adaptive Fuzzy Leader–Follower Synchronization of Constrained Heterogeneous Multiagent Systems. *IEEE Trans. Fuzzy Syst.* **2022**, *30*, 205–219.
19. Rojsiraphisal, T.; Mobayen, S.; Asad, J.H.; Vu, M.T.; Chang, A.; Puangmalai, J. Fast Terminal Sliding Control of Underactuated Robotic Systems Based on Disturbance Observer with Experimental Validation. *Mathematics* **2021**, *9*, 1935. [CrossRef]
20. Wang, D.; Huang, J. Neural network-based adaptive dynamic surface control for a class of uncertain nonlinear systems in strict-feedback form. *IEEE Trans. Neural Netw.* **2005**, *16*, 195–202.
21. Zhou, Q.; Wu, C.; Jing, X.; Wang, L. Adaptive fuzzy backstepping dynamic surface control for nonlinear Input-delay systems. *Neurocomputing* **2016**, *199*, 58–65. [CrossRef]
22. Wu, J.; Chen, X.; Zhao, Q.; Li, J.; Wu, Z.G. Adaptive Neural Dynamic Surface Control with Prespecified Tracking Accuracy of Uncertain Stochastic Nonstrict-Feedback Systems. *IEEE Trans. Cybern.* **2022**, *52*, 3408–3421. [CrossRef]
23. Zhang, T.; Xia, M.; Yi, Y.; Shen, Q. Adaptive Neural Dynamic Surface Control of Pure-Feedback Nonlinear Systems with Full State Constraints and Dynamic Uncertainties. *IEEE Trans. Syst. Man, Cybern. Syst.* **2017**, *47*, 2378–2387. [CrossRef]
24. Charfeddine, S.; Boudjemline, A.; Ben Aoun, S.; Jerbi, H.; Kchaou, M.; Alshammari, O.; Elleuch, Z.; Abbassi, R. Design of a Fuzzy Optimization Control Structure for Nonlinear Systems: A Disturbance-Rejection Method. *Appl. Sci.* **2021**, *11*, 2612. [CrossRef]
25. Zhu, Z.; Xia, Y.; Fu, M. Attitude stabilization of rigid spacecraft with finite-time convergence. *Int. J. Robust Nonlinear Control* **2011**, *21*, 686–702. [CrossRef]
26. Polyakov, A. Nonlinear Feedback Design for Fixed-Time Stabilization of Linear Control Systems. *IEEE Trans. Autom. Control* **2012**, *57*, 2106–2110. [CrossRef]
27. Ni, J.; Ahn, C.K.; Liu, L.; Liu, C. Prescribed performance fixed-time recurrent neural network control for uncertain nonlinear systems. *Neurocomputing* **2019**, *363*, 351–365. [CrossRef]

28. Hu, X.; Li, Y.X.; Hou, Z. Event-Triggered Fuzzy Adaptive Fixed-Time Tracking Control for Nonlinear Systems. *IEEE Trans. Cybern.* **2022**, *52*, 7206–7217. [CrossRef]

29. Sun, J.; Pu, Z.; Yi, J.; Liu, Z. Fixed-Time Control With Uncertainty and Measurement Noise Suppression for Hypersonic Vehicles via Augmented Sliding Mode Observers. *IEEE Trans. Ind. Inform.* **2020**, *16*, 1192–1203. [CrossRef]

30. Wang, L.; Chen, C.L.P.; Li, H. Event-Triggered Adaptive Control of Saturated Nonlinear Systems with Time-Varying Partial State Constraints. *IEEE Trans. Cybern.* **2020**, *50*, 1485–1497. [CrossRef]

31. Zhou, Q.; Li, H.; Wu, C.; Wang, L.; Ahn, C.K. Adaptive Fuzzy Control of Nonlinear Systems with Unmodeled Dynamics and Input Saturation Using Small-Gain Approach. *IEEE Trans. Syst. Man Cybern. Syst.* **2017**, *47*, 1979–1989. [CrossRef]

32. Min, H.; Xu, S.; Ma, Q.; Zhang, B.; Zhang, Z. Composite-Observer-Based Output-Feedback Control for Nonlinear Time-Delay Systems with Input Saturation and Its Application. *IEEE Trans. Ind. Electron.* **2018**, *65*, 5856–5863. [CrossRef]

33. Wang, L.; Li, H.; Zhou, Q.; Lu, R. Adaptive Fuzzy Control for Nonstrict Feedback Systems with Unmodeled Dynamics and Fuzzy Dead Zone via Output Feedback. *IEEE Trans. Cybern.* **2017**, *47*, 2400–2412. [CrossRef]

34. Zhang, L.; Yang, G.H. Adaptive Fuzzy Prescribed Performance Control of Nonlinear Systems with Hysteretic Actuator Nonlinearity and Faults. *IEEE Trans. Syst. Man Cybern. Syst.* **2018**, *48*, 2349–2358. [CrossRef]

35. Liu, Z.; Lai, G.; Zhang, Y.; Chen, X.; Chen, C.L.P. Adaptive Neural Control for a Class of Nonlinear Time-Varying Delay Systems with Unknown Hysteresis. *IEEE Trans. Neural Netw. Learn. Syst.* **2014**, *25*, 2129–2140.

36. Sanner, R.M.; Slotine, J.J.E. Gaussian networks for direct adaptive control. *IEEE Trans. Neural Netw.* **1992**, *3*, 837–863. [CrossRef]

37. Wang, F.; Lai, G. Fixed-time control design for nonlinear uncertain systems via adaptive method. *Syst. Control Lett.* **2020**, *140*, 104704. [CrossRef]

38. Hardy, G.H.; Littlewood, J.E.; Pólya, G. *Inequalities*; Cambridge University Press: Cambridge, UK, 1952.

39. Zhou, Z.; Tong, D.; Chen, Q.; Zhou, W.; Xu, Y. Adaptive NN control for nonlinear systems with uncertainty based on dynamic surface control. *Neurocomputing* **2021**, *421*, 161–172. [CrossRef]